Assigning UPDRS Scores in the Leg Agility Task of Parkinsonians: Can It Be Done Through BSN-Based Kinematic Variables?

Matteo Giuberti, *Member, IEEE*, Gianluigi Ferrari, *Senior Member, IEEE*, Laura Contin, Veronica Cimolin, Corrado Azzaro, Giovanni Albani, and Alessandro Mauro

Abstract—In this paper, by characterizing the leg agility (LA) task, which contributes to the evaluation of the degree of severity of the Parkinson's disease (PD), through kinematic variables (including the angular amplitude and speed of thighs' motion), we investigate the link between these variables and unified Parkinson's disease rating scale (UPDRS) scores. Our investigation relies on the use of a few body-worn wireless inertial nodes and represents a first step in the design of a portable system, amenable to be integrated in Internet of Things (IoT) scenarios, for automatic detection of the degree of severity (in terms of UPDRS score) of PD. The experimental investigation is carried out considering 24 PD patients.

Index Terms—Inertial sensors, leg agility (LA), Parkinson's disease (PD), unified Parkinson's disease rating scale (UPDRS) scores.

I. INTRODUCTION

A. Motivation

PARKINSON's disease (PD) is the second most common neurodegenerative disorder after Alzheimer's disease. According to the global declaration for PD, 6.3 million people suffer from PD worldwide [1]. The prevalence of PD is about 0.3% of the whole population in industrialized countries, rising up to 1% over the age of 65 and to 4% over 80.

The clinical picture of PD is characterized by a progressive deterioration of the motor performance, with the occurrence of slowness (bradykinesia) and poverty of voluntary movements, expressionless face, "resting" tremor, stooped posture, festinating gait, and axial instability. Asymmetry of motor symptoms is a typical feature of PD. Although the symptoms can be improved by dopaminergic drugs, such as L-dopa, over time its effectiveness worsens and motor fluctuations may occur as well as dyskynesias and involuntary movements. Furthermore, variations in the severity of these symptoms are observed during dosing intervals.

The clinical picture assessed during an outpatient check up in the medical office poorly represents the real (actual) clinical status, especially in fluctuating patients. Indeed, repeated daily assessments of motor symptoms would be required and this is usually done by asking the patient to annotate the number of hours of OFF (i.e., when drugs are not effective) and ON condition (i.e., when they are effective), but this is not fully reliable due to perceptual bias. For this reason, in recent years, a number of studies on automatic systems to evaluate motor fluctuations of PD patients have been developed [2]. The most common approach is leveraging sensing technology to automatically evaluate the performance of specific motor tasks, such as "sit-to-stand" [3], [4], gait analysis [5], [6], and tremor [7]. The basic idea is to develop a system able to get an evaluation of the motor status of a patient as close as possible to the evaluation of neurologists when they apply semiquantitative evaluation scales, such as the unified Parkinson's disease rating scale (UPDRS) [8].

B. Leg Agility Task

Although several works have appeared focusing on the evaluation of the performance of specific motor tasks, such as "sit-to-stand" [3], [4], gait analysis [5], [6], and tremors [7], to the best of our knowledge, limited attention has been devoted, in the literature, to the evaluation of the leg agility (LA) task [9]–[13].

1) Task description: The LA task aims at evaluating the severity of motion impairments of a PD patient, with specific focus on the lower limbs. In this exercise, the patient is asked to sit on a chair provided with rigid backrest and armrests. The patient must place both his/her feet on the floor in a comfortable position. The exercise consists in alternately raising up and stomping the feet on the ground, as high and as fast as possible.

TABLE I
UPDRS MAPPING

UPDRS	Amplitude	Slowing	Hesitations	Interruptions	Freezing
0	Nearly constant	No	0	0	0
1	Decrements near the end	Slight	≥ 1	1,2	0
2	Decrements midway	Mild	–	3,4,5	0
3	Decrements after first tap	Moderate	–	≥ 6	≥ 1
4	Always minimal or null	Severe	–	Always	–

Ten repetitions per leg must be performed while sitting on the chair in order to test each leg separately. The examiner should first train the patient, showing him/her the correct execution of the exercise, stopping as soon as the patient starts. The significant parameters that have to be measured, independently for each leg, are the speed, the regularity, and the amplitude of the movement. Moreover, differences can be observed between the movements performed with the different legs. For this reason, in the following, we will distinguish between right LA (RLA) and left LA (LLA) tasks.

2) UPDRS Evaluation: According to the guidelines of the Movement Disorder Society (MDS), the LA task must be evaluated observing the following parameters: amplitude, slowing, hesitations, interruptions, and freezing. In particular, in Table I, an attempt at mapping these parameters with an UDPRS evaluation is presented. To this end, note that UPDRS scores are integer values that range from 0 (no problems) to 4 (worst conditions). While the first feature (i.e., amplitude) directly corresponds to a physical measure, the quantitative evaluation of the other ones typically relies on the experience of neurologists. Therefore, inter-neurologist score variations cannot be *a priori* excluded.

C. Paper Contribution

In this work, we focus on the characterization of the LA task in PD patients, devising an approach for quantitative evaluation of relevant kinematic features representative of the UPDRS score of a patient. This work extends the preliminary results presented in [12] and [13], including also a novel frequency domain analysis, which allows to identify more accurately relevant kinematic features representative of the UPDRS level. After showing, with direct comparison with an optoelectronic system, that the LA task can be effectively characterized by analyzing the inclination and angular velocity of the thighs, we characterize the kinematic variables associated with the thighs' motion. We first present a "single subject" experimental characterization the LA task, comparing directly a healthy patient with a PD patient, highlighting similarities and differences. Then, we perform a "large-scale" (considering 24 PD patients) experimental analysis, identifying the most significant kinematic features associated with the LA task characterization, by mapping them with the UPDRS scores attributed by expert neurologists. The encouraging experimental results, suggesting that the UPDRS score might be concisely characterized (e.g., as a decreasing function of the "power" of a movement), motivate the design and implementation of an automatic UPDRS detection system based on the use of a few body-worn inertial sensors. Moreover, the use of wireless inertial sensors makes such a portable system easily integrable in Internet of Things (IoT) scenarios, allowing directly remote monitoring and data sharing.

D. Paper Structure

This paper is organized as follows. Section II describes the experimental setup, detailing the used hardware and the considered subjects (both Parkinsonians and healthy). In Section III, the LA task is characterized by, first, showing the equivalence between heel elevation (as measured with an optoelectronic system) and thigh inclination (as measured with the wireless inertial sensor-based system) and then, by extracting relevant kinematic features, in both time and frequency domains. In Section IV, the obtained experimental results are presented and commented. Finally, Section V concludes this paper.

II. EXPERIMENTAL SETUP

A. Hardware Description

The experiments were carried out at the San Giuseppe Hospital, Istituto Auxologico Italiano, in Piancavallo (Verbania, Italy), at a fully equipped last generation motion analysis laboratory. In particular, the kinematic analysis was carried out, in a comparative way, considering 1) an optoelectronic system; and 2) a wireless body sensor network (BSN)-based system, based on a few nodes (equipped with inertial and magnetic sensors) placed over the body.

The optoelectronic system (Vicon, Oxford, UK) performs a real-time processing of images from six fixed infrared cameras (with sampling rate equal to 100 Hz) to extract the reflectance of passive markers (with a diameter of 0.015 m), which are positioned on specific anatomical landmarks of the subject. Prior to testing, the system was calibrated to assure accuracy and to allow the computation of each marker's 3-D coordinates. The average error on the computation of the difference between measured and actual distances of two markers fixed at the edges of a rigid bar was within 0.00021 m (with standard deviation equal to 0.0001 m). The calibrated volume for this application had: length equal to 3.5 m (x-axis of the laboratory reference system); height equal to 2 m (y-axis of the laboratory reference system); and width equal to 2 m (z-axis of the laboratory reference system).

The BSN is formed by Shimmer (sensing health with intelligence, modularity, mobility, and experimental reusability) nodes [14]. A Shimmer node is a small and low-power wireless sensing platform that can capture and communicate a wide range of sensed data in real time. The main module is a compact

TABLE II
CONSIDERED SUBJECTS FOR A DIRECT (ONE-TO-ONE) COMPARISON BETWEEN PD AND HEALTHY SUBJECTS

Subject	Sex	Age	Weight (kg)	Height (m)	UPDRS score for LA	Exercises
A (healthy)	Female	40	56	1.71	0	1xRLA, 1xLLA
B (PD)	Male	42	85	1.80	1 (bilaterally)	1xRLA, 1xLLA

wearable device (size: 0.053 m × 0.032 m × 0.025 m; weight: 0.022 kg) equipped with: a TI MSP430 microcontroller; a bluetooth radio (roving networks RN-42) and an IEEE 802.15.4 compliant radio (TI CC2420); an integrated 2 GB microSD card slot; a 450 mAh rechargeable Li-ion battery; and a triaxial accelerometer (freescale MMA7361). Moreover, the device is designed so that different external sensing modules can be easily connected. In particular, the 9DoF kinematic sensor expansion module, which is supplied with a triaxial gyroscope (InvenSense 500 series) and a triaxial magnetometer (Honeywell HMC5843), has been used.

B. Subjects

1) Single-Subject Analysis: We first evaluated the LA tasks performed by two individuals: 1) healthy subject (subject A); and 2) a PD patient (subject B). Subject B has a disease duration of 4 years and does not present motor fluctuations. His Hoehn & Yahr score was 2 and the UPDRS score for LA was 1 bilaterally. The score of 1 was assigned because of the presence of one hesitation of the movement and a slight slowing during the limb motion. In Table II, we summarize the data of the considered subjects, indicating also the performed exercises.

2) Large-Scale Analysis: The large-scale experimental results carried out for this work refer to a group of 24 PD patients (17 males and 7 females) with age ranging from 31 years to 79 years (with mean equal to 65.9 years and standard deviation equal to 12.3 years). The patients have been asked to perform 10 repetitions of LA per leg, providing them instructions as described in Section I-B1. A total of 72 LA trials (which comprise 36 RLA and 36 LLA) have been collected.[1] The patients' UPDRS scores, assigned by neurologists, ranged from 0 to 3.5. To this end, note that, unlike what the MDS document indicates, noninteger (∗.5-type) scores have also been used in the case of indecision between two consecutive integer UPDRS values. In particular, the distribution of the 76 UPDRS scores assigned to the considered LA trials is shown in Fig. 1.

C. Acquisition and Optoelectronic Validation

As anticipated in Section II-A, spatial and temporal parameters, along with the kinematic of the user lower limbs, have been monitored and evaluated using the considered BSN-based inertial system and a reference optoelectronic system. Specifically, the optoelectronic system has been used to estimate the 3-D position of passive markers positioned on specific anatomical landmarks of the subject. Passive markers data were collected on all body segments (pelvis, thigh, shank, and foot bilaterally).

[1]Note that, even if only 24 patients have been considered, some patients have performed the LA task multiple times, at different times and/or for different PD conditions.
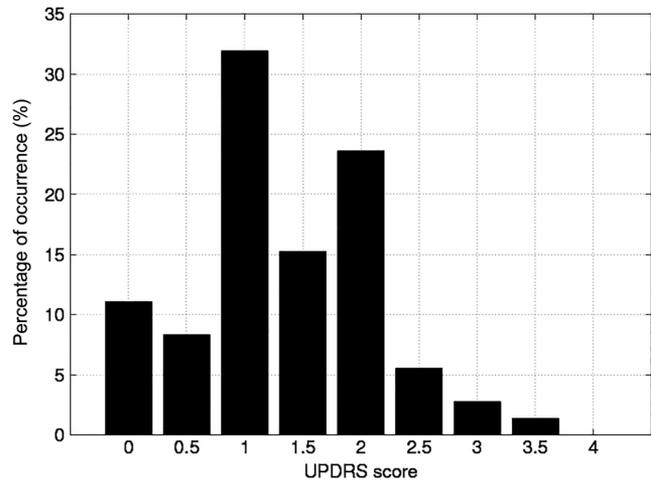

Fig. 1. Distribution of the 76 UPDRS scores assigned to the LA trials considered in the experimental analysis.
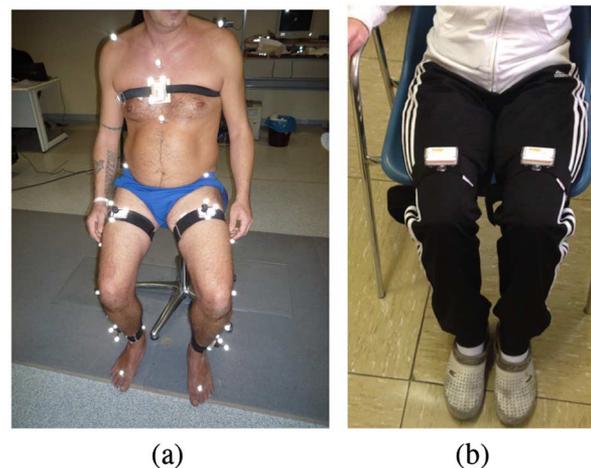

(a) (b)

Fig. 2. Overview of the experimental testbed applied to a monitored subject. (a) Configuration for single-subject optoelectronic validation. (b) Final configuration for large-scale analysis.

The Davis marker-set was chosen as the protocol of choice to acquire the motion of lower limbs and trunk based on [15] and [16].

Concerning the inertial system, a Shimmer node (with sampling rate equal to 102.4 Hz) has been attached to each thigh of the monitored user with Velcro straps. The Shimmer devices have been placed trying to align the plane defined by the x- and y-axes of the device with the frontal plane of the user and trying to align one of the two axes with the direction of the femur. For ease of clarity, the placement of Shimmer nodes on the patient thighs is shown in Fig. 2.

In addition to the markers specified in the Davis protocol, two groups of three markers are mounted on two frames fixed

Fig. 3. Three orthogonally positioned reflective markers positioned over a Shimmer node.

on two Shimmer devices (for a total of six additional markers). The three reflective markers are fixed on each Shimmer device through a frame of orthogonal rods of equal lengths (aligned, as precisely as possible, with the reference system of the Shimmer device), as shown in Fig. 3. The estimation of the 3-D positions of the markers of a frame (with the optoelectronic system) allows to estimate the reference orientation of the device, which is used as ground truth for the actual Shimmer orientation. We remark that, because of imperfections in the frame design (i.e., the rods could not be perfectly orthogonal or have the same lengths), a "best-fit" orientation is estimated [17]. Furthermore, due to a possible misalignment between the Shimmer reference system and the frame, a calibration step is performed once (at the beginning of each exercise) in order to estimate the fixed rotation between the two reference systems. This rotation is then applied to align the following measurements.

Finally, the inertial and optoelectronic systems (which are already independently synchronized) are jointly synchronized by computing the angular velocity of every optical frame and comparing it with the angular velocity measured by the corresponding Shimmer. The estimated time shift value is determined as the one which maximizes the correlation of the two signals.

III. Leg Agility Characterization

A. Equivalence Between Heel Elevation and Thigh Inclination: Optoelectronic Validation

According to the guidelines of the MDS, the LA task of the UPDRS should be evaluated by observing specific significant variables. As an example, the amplitude of the heel elevation and the speed of each repetition should be monitored, specifically focusing on their variations along the duration of the exercise. Furthermore, hesitations, interruptions, and freezing of the movement should also be evaluated. As shown in Table I, general rules can be easily constructed in order to define an unambiguous mapping between observed variables and UPDRS scores.

These variables can be quite easily extracted from optical data just observing the estimated 3-D positions of each marker placed on the subjects' heels (one per heel) and, in particular, its "vertical" component, denoted as z_H [dimension: (m)],

which then indicates its elevation. To this end, a segmentation of the LA data, manually performed upon frame-by-frame observation of the videos recorded for each session, is necessary. Hesitations, interruptions, and freezing of the movement are more difficult to define but they can generally be associated with sudden variations, fluctuations, or pauses in z_H and in the linear "vertical" velocity $v_H \triangleq dz_H/dt$ [dimension: (m/s)].

First, we show that, in order to analyze the LA task, it is sufficient to consider the Shimmer nodes positioned over the thighs. In order to do this, we verify that the analysis of thighs' kinematic (measured through the inertial system) is actually equivalent to that of the heels' kinematic (measured through the optoelectronic system).

To this end, the 3-D orientation of a Shimmer device is estimated through an orientation filter, based on a gradient descent algorithm, which properly weighs the measurements of the three sensors of the Shimmer (i.e., accelerometer, gyroscope, and magnetometer) [18]. The inclination θ [dimension: (deg)] of the thigh is then computed as the angle between the Shimmer axis (parallel to the femur direction) and the world vertical axis, reduced by 90°—this is expedient to measure 0° when the subject is sitting. Moreover, the angular velocity of the thighs, directly measured through the Shimmer's gyroscope, is considered. In particular, we define as ω [dimension: (deg/s)] the component of the angular velocity measured around the Shimmer axis perpendicular to the femur direction and lying in the frontal plane of the user.

At this point, z_H is compared to θ and v_H is compared to ω. For both subjects A and B introduced in Section II-B1, the correlation between z_H and θ is between 0.98 and 0.99 and the correlation between v_H and ω is between 0.93 and 0.98, respectively, showing then a strong correlation between heels' optical data and thighs' inertial data—no graph is shown for lack of space. Therefore, this motivates the use, in the following analysis, of the signals extracted from the Shimmer nodes of the thighs, i.e., θ and ω.

In order to highlight the accuracy of the estimation of the thigh inclination θ provided by the orientation filter acting on Shimmer data, a direct comparison between the inclination estimated through the optoelectronic system (by means of the orthogonal frame of markers shown in Fig. 3) and that estimated through the inertial sensor has been performed, showing an average root-mean-square error (RMSE) of 1.75° (with a standard deviation of 1.32°). For the sake of clarity, in Fig. 4, the thigh inclination θ, estimated using both the inertial and the optical systems, is also shown for an illustrative LA trial. It is easy to see that, even if the subject movement presents a high dynamicity, the error between the inclination measured with the two systems is almost negligible. Therefore, the analysis conducted in the following will be based on inertial data.

B. LA Features in the Time Domain

Upon frame-by-frame observation of the videos recorded for each session (execution of the LA task by a patient), the inclination signals have been manually segmented in order to extract information about single repetitions within the LA task. This segmentation allows to define three time labels, denoted as
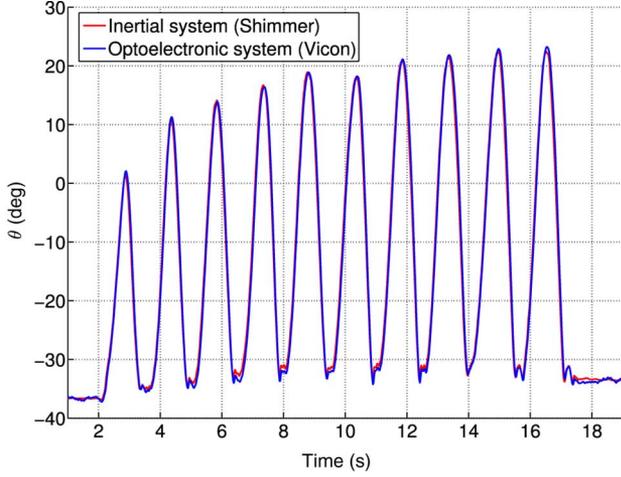
Fig. 4. Direct comparison between the inclinations estimated through opto-electronic (Vicon) and inertial (Shimmer) systems for an illustrative LA trial.
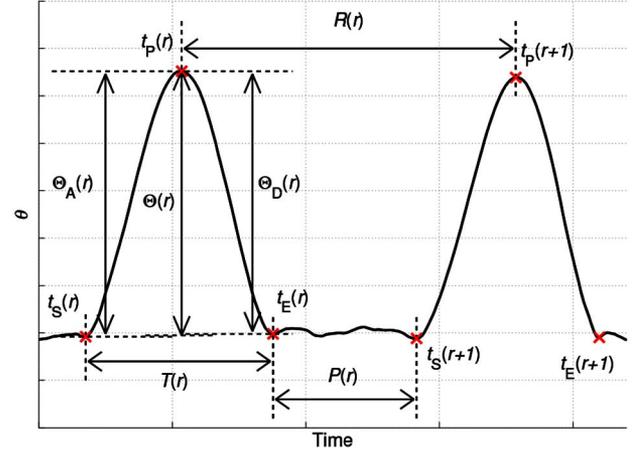

Fig. 5. Graphically intuitive representation of some of the involved kinematic variables. Two illustrative consecutive repetitions of LA are shown together with the corresponding segmentation events (red crosses).

$t_S(r)$, $t_E(r)$, and $t_P(r)$, associated, respectively, with the start, the end, and the epoch of maximal thigh inclination of the rth LA repetition ($r \in \{1, 2, \ldots, 10\}$).

Starting from the previous labels and the inclination signal, for each repetition r ($r \in \{1, 2, \ldots, 10\}$) of the LA (either RLA or LLA) the following features, relative to the time domain, can be straightforwardly computed.

1) The angular amplitude $\Theta(r)$ [dimension: (deg)]

$$\Theta(r) \triangleq \frac{\Theta(r) + \Theta(r)}{2}$$

where

$$\Theta_A(r) \triangleq \theta(t_P(r)) - \theta(t_S(r)) \tag{1}$$

$$\Theta_D(r) \triangleq \theta(t_P(r)) - \theta(t_E(r)). \tag{2}$$

2) The angular speed of execution $\Omega(r)$ [dimension: (deg/s)]

$$\Omega(r) \triangleq \frac{\Theta_A(r) + \Theta_D(r)}{T(r)} = \frac{\Theta_A(r) + \Theta_D(r)}{t_E(r) - t_S(r)}.$$

Furthermore, for each pair of consecutive repetitions, say r and $r+1$ ($r \in \{1, \ldots, 9\}$), of the LA (either RLA or LLA) the following features can be computed.

1) The rth pause of execution $P(r)$ [dimension: (s)]

$$P(r) \triangleq t_S(r+1) - t_E(r).$$

2) The rth regularity of execution $R(r)$ [dimension: (s)]

$$R(r) \triangleq t_P(r+1) - t_P(r).$$

For ease of clarity, in Fig. 5, some of the just introduced kinematic variables are shown for two illustrative consecutive repetitions of LA, say r and $r+1$. Finally, if we jointly consider the RLA and the LLA repetitions of the same patient, for each repetition r ($r \in \{1, 2, \ldots, 10\}$) of the LA, the following features can also be computed.

1) The relative difference of the angular amplitude between LLA and RLA $D_{\Theta,\mathrm{LR}}(r)$ [adimensional: (%)]

$$D_{\Theta,\mathrm{LR}}(r) \triangleq \frac{\Theta_{\mathrm{LLA}}(r) - \Theta_{\mathrm{RLA}}(r)}{\Theta_{\mathrm{RLA}}(r)} \cdot 100.$$

2) The relative difference of the angular speed between LLA and RLA $D_{\Omega,\mathrm{LR}}(r)$ [adimensional: (%)]

$$D_{\Omega,\mathrm{LR}}(r) \triangleq \frac{\Omega_{\mathrm{LLA}}(r) - \Omega_{\mathrm{RLA}}(r)}{\Omega_{\mathrm{RLA}}(r)} \cdot 100.$$

Since a single LA repetition may lead to misleading indications about the execution of the whole LA task, the following average features (obtained by averaging, over consecutive repetitions, the features introduced above) are considered in the following experimental analysis[2]:

$$\Theta \triangleq \frac{\sum_{r=1}^{10} \Theta(r)}{10} \quad \Omega \triangleq \frac{\sum_{r=1}^{10} \Omega(r)}{10}$$

$$P \triangleq \frac{\sum_{r=1}^{9} P(r)}{9} \quad R \triangleq \frac{\sum_{r=1}^{9} R(r)}{9}$$

$$D_{\Theta,\mathrm{LR}} \triangleq \frac{\sum_{r=1}^{10} D_{\Theta,\mathrm{LR}}(r)}{10} \quad D_{\Omega,\mathrm{LR}} \triangleq \frac{\sum_{r=1}^{10} D_{\Omega,\mathrm{LR}}(r)}{10}.$$

In addition, the following standard deviations (with the same dimensions) of some of the previous features are also considered:

$$\Theta_{\mathrm{SD}} \triangleq \sqrt{\frac{\sum_{r=1}^{10} (\Theta(r) - \Theta)^2}{9}} \quad \Omega_{\mathrm{SD}} \triangleq \sqrt{\frac{\sum_{r=1}^{10} (\Omega(r) - \Omega)^2}{9}}$$

$$P_{\mathrm{SD}} \triangleq \sqrt{\frac{\sum_{r=1}^{9} (P(r) - P)^2}{8}} \quad R_{\mathrm{SD}} \triangleq \sqrt{\frac{\sum_{r=1}^{9} (R(r) - R)^2}{8}}.$$

We also introduce the repetition frequency F [dimension: (Hz)], defined as follows:

$$F \triangleq \frac{10}{t_E(10) - t_S(1)}.$$

[2]From a notation viewpoint, the symbols used for average features are the same of those of repetition-based features, but the dependence from r disappears.
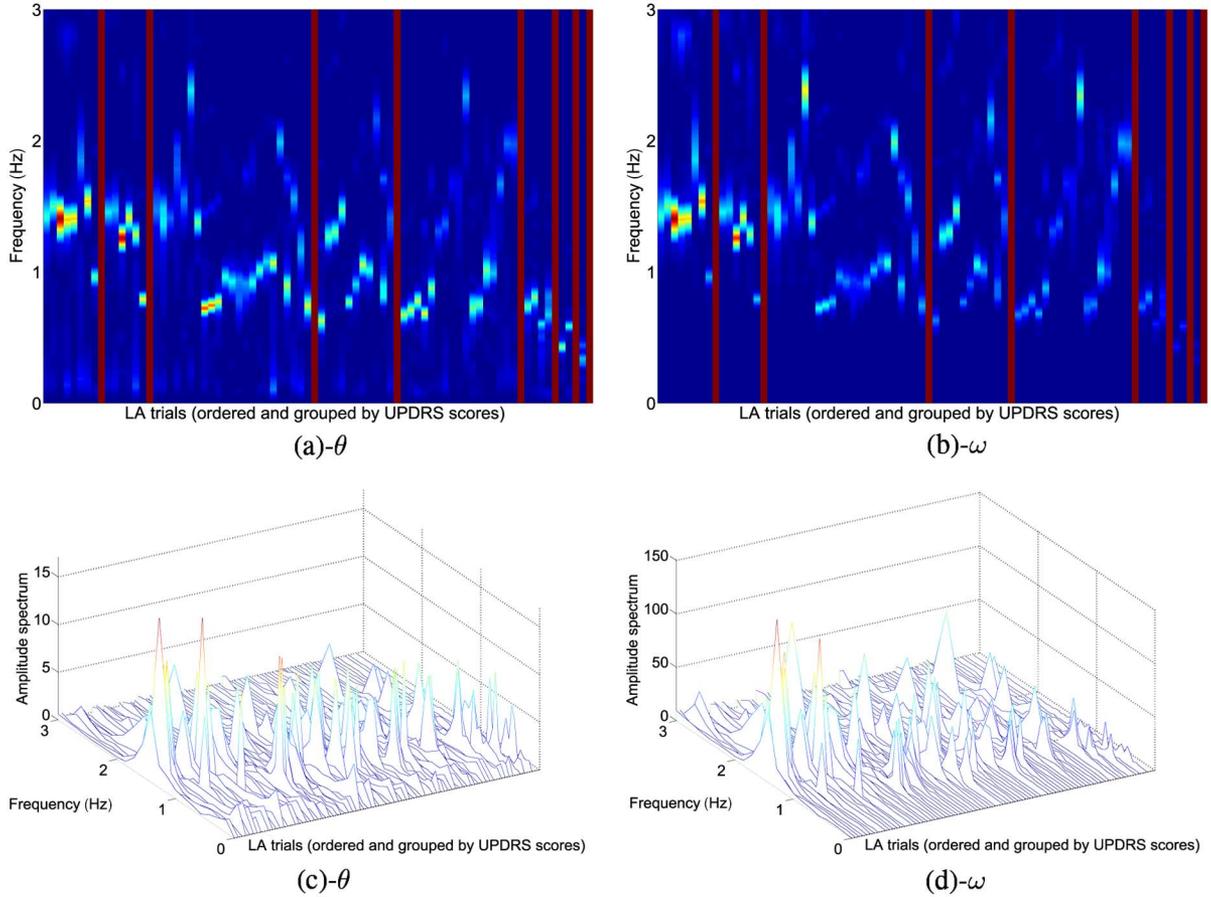
Fig. 6. One-sided amplitude spectra of θ (i.e., inclination of the thigh) and ω (i.e., angular velocity of the thigh) for different LA trials: (a) and (b) 2-D and (c) and (d) 3-D representations. Magnitudes of the spectra are mapped to a color that ranges from blue (lowest values) to red (highest values). The LA trials are ordered and grouped by UPDRS scores (from 0 to 3.5). Groups of spectra corresponding to different UPDRS scores are separated either (a) and (b) using a vertical red line or (c) and (d) skipping a line in the graphs.

Note that, for each LA trial, two values of Θ, Ω, P, R, and F are computed (namely, one for the RLA and one for the LLA), whereas only one value of $D_{\Theta,\text{LR}}$ and $D_{\Omega,\text{LR}}$ is computed.[3]

C. Leg Agility Features in the Frequency Domain

While the features considered in Section III-B belong to the time domain, we now focus on the characterization of the LA task by extracting relevant information on the UPDRS value in the frequency domain.

For the following frequency analysis, the signals $\theta(t)$ (i.e., the inclination of the thighs) and $\omega(t)$ (i.e., the angular velocity of the thighs), introduced in Section III-A, are considered. Specifically, the latter is directly measured through the Shimmer gyroscope and is defined as the component of the angular velocity measured around the Shimmer axis perpendicular to the femur direction and lying in the frontal plane of the user. The considered signals θ and ω are properly segmented in order to start at the initial instant of the first LA repetition and to end at the final instant of the last LA repetition.

[3]In the large-scale analysis considered in Section IV-B, 72 values of Θ, Ω, P, R, and F will be available, whereas 36 values of $D_{\Theta,\text{LR}}$, and $D_{\Omega,\text{LR}}$ will be available. Finally, a UPDRS score $u \in \{0, 0.5, 1, 1.5, 2, 2.5, 3, 3.5, 4\}$ will be assigned to each of the 72 LA trials.

The spectra [namely, the discrete Fourier transforms, (DFTs)] of θ and ω (properly centered on their means) have been computed using a fast Fourier transform (FFT) algorithm for every leg of every patient. More formally, denoting $x \in \{\theta, \omega\}$, the hth component of the spectrum X_{FFT} of the signal x is computed as follows:

$$X_{\text{FFT},h} = \sum_{n=0}^{N-1} x_n e^{-jh\frac{2\pi}{N}n}, \qquad h = 0, \ldots, N-1 \quad (3)$$

where N is the length of x (and, consequently, the length of $X_{\text{FFT},h}$). The amplitude spectrum (which we will just consider in the following) is then easily computed by dividing the absolute value of X_{FFT} by N

$$X = \frac{|X_{\text{FFT}}|}{N}. \quad (4)$$

The obtained spectra have been then grouped and ordered according to the UPDRS score of the corresponding patient. All the computed spectra of θ and ω are shown, using a one-sided representation, in Fig. 6. For these spectra, both 2-D [(a) and (b)] and 3-D [(c) and (d)] representations are provided. It may be observed that the spectra amplitudes for both θ and ω generally decrease moving from low UPDRS scores to higher ones.
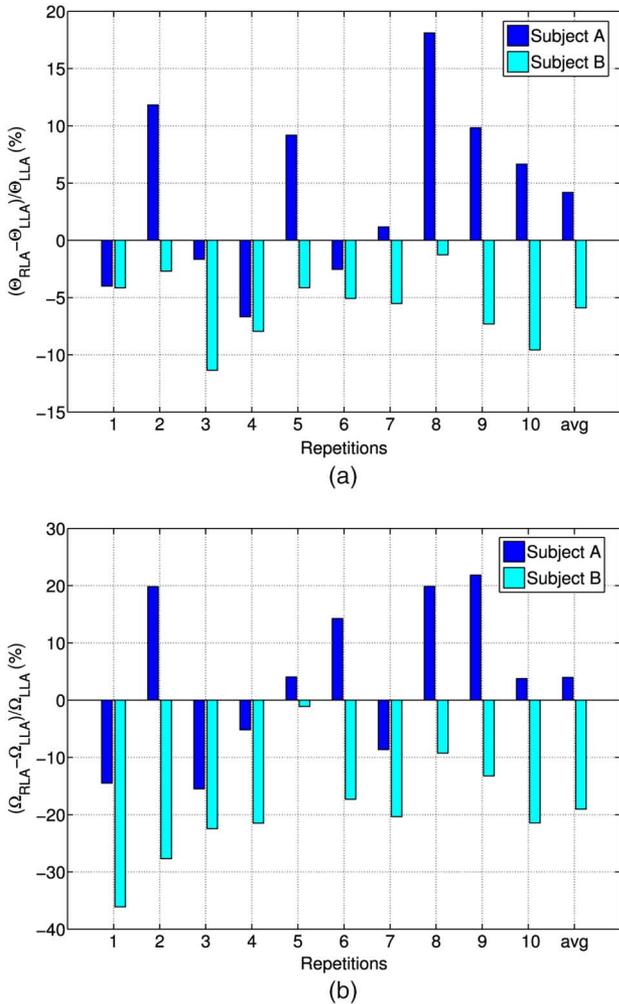
Fig. 7. Comparison, over ten repetitions, between Subject A (healthy) and Subject B (PD), in terms of: (a) relative angular amplitude difference (percentage) between the two legs and (b) relative angular speed difference (percentage) between the two legs.

To this end, in our analysis, we will take into account a new feature, i.e., the spectrum power. More formally, for the spectrum X, its power P_X is computed as follows:

$$P_X = \frac{1}{N} \sum_{h=0}^{N-1} (X_h)^2. \tag{5}$$

In the following, for ease of understanding when X is the spectrum of either θ or ω, the used notation will be X_θ or X_ω, respectively.

IV. RESULTS AND DISCUSSION

A. Single-Subject Analysis

First, we analyze the amplitude and the speed of each repetition, indicated in the MDS's UPDRS document as the main variables to be observed in the LA task. In Fig. 7(a), the difference in angular amplitude, expressed in percentage, is shown for each repetition (from 1 to 10), comparing directly Subjects A and B. It can be noticed that Subject A does not present a biased difference between RLA and LLA, whereas Subject B's

RLA angular amplitude is always lower than that of LLA. On average, it can be observed that the relative difference between RLA and LLA is around 4% for Subject A and around 6% for Subject B. Similarly, the difference (expressed in percentage) between the RLA and LLA angular speeds, shown in Fig, 7(b), reveals that Subject B's RLA angular speed is 19% lower than his LLA angular speed. On the contrary, this is generally not true for Subject A, for which the relative difference is, on average, around 4%.

According to the results in Fig. 7, it is worth to highlight that the difference observed between the RLA and the LLA of a specific subject, even if not specifically referenced in the MDS's document as a significant variable, can instead represent a clear evidence of a nonzero UPDRS score. Therefore, a possible extension of the UPDRS can already be envisioned just by introducing this new variable in the LA analysis.

In order to better investigate and characterize the LA repetitions, a qualitative analysis has been carried out by investigating the angular velocity ω along an entire repetition. In particular, in Fig. 8, the segmented portions of ω, corresponding to each LA repetition, have been normalized in time and value (so that time goes from 1 to 100 and $-1 \le \omega \le +1$) and overlapped for (a) Subject A and (b) Subject B, respectively. Even if both subjects show some macrohesitations (specifically when raising up the heels), it is easy to see that Subject B's angular velocity presents several microhesitations, not easily observable, with a naked eye, in recorded videos. This can be then another useful kinematic aspect to be taken into account in order to better investigate the LA task and predict the presence of PD.

B. Large-Scale Analysis

As anticipated in Section I-C, the aim of the following analysis is to devise an approach to automatically assign a UPDRS score to a specific LA task. To this end, it is crucial to determine if there exists a relationship between the UPDRS score assigned by neurologists to an LA task and the values of the kinematic variables introduced in Section III. In particular, our goal is to determine if there exist UPDRS "trajectories," in the kinematic (multidimensional) feature space, which clearly allow to detect the correct UPDRS value.

In Fig. 9, all the average amplitude-speed pairs $\{(\Theta_i, \Omega_i)\}_{i=1}^{72}$ are represented on the same plane. Each pair is assigned a color corresponding to the related UPDRS score. Furthermore, the centroids (denoted by the filled stars) of each cluster of pairs, corresponding to the same UPDRS score, are also shown. Finally, the black line links the centroids from 0 to 3.5 (in addition, a representative red arrow shows a smoothed version of this trajectory). It can be observed that uniform clusters of pairs with same UPDRS scores are highly distinguishable for very low and very high UPDRS scores. Furthermore, even if clusters of pairs corresponding to different UPDRS scores tend to overlap, a clear trend is visible showing that pairs mainly move from the upper right corner (i.e., the pairs with UPDRS 0) to the bottom part (i.e., the pair with UPDRS 3.5) of the plane. This also supports the intuition that amplitude and speed of motion are mostly correlated.
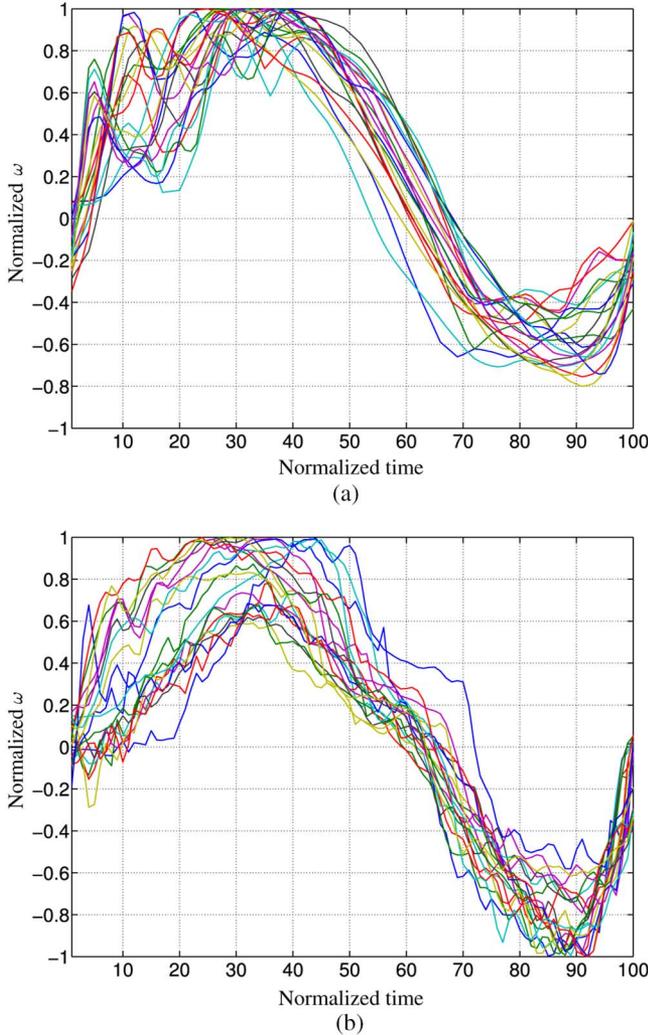
(a)

(b)

Fig. 8. Juxtaposed normalized (between ± 1) angular velocities ω of 10 repetitions, normalized over time (between 1 and 100) for: (a) Subject A and (b) Subject B.
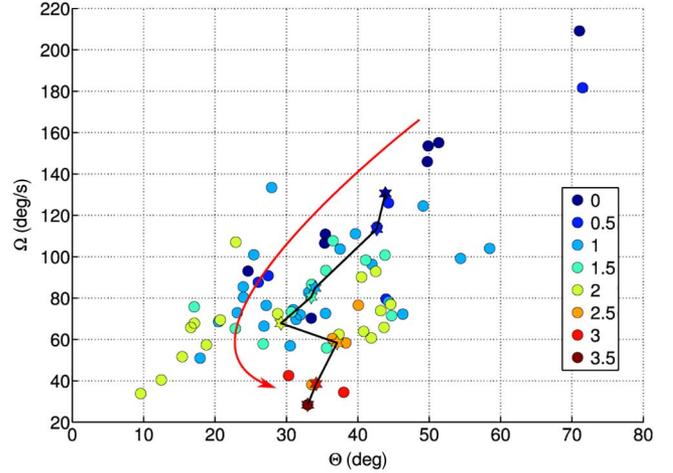

Fig. 9. Representation of average amplitude-speed pairs $\{(\Theta_i, \Omega_i)\}_{i=1}^{72}$ on the same plane. Pairs are colored according to the corresponding UPDRS scores. Centroids of each cluster of pairs (drawn as filled stars), corresponding to the same UPDRS score, are shown and are linked in UPDRS-wise order from 0 to 3.5. For ease of clarity, a representative red arrow shows a smoothed version of this trajectory.
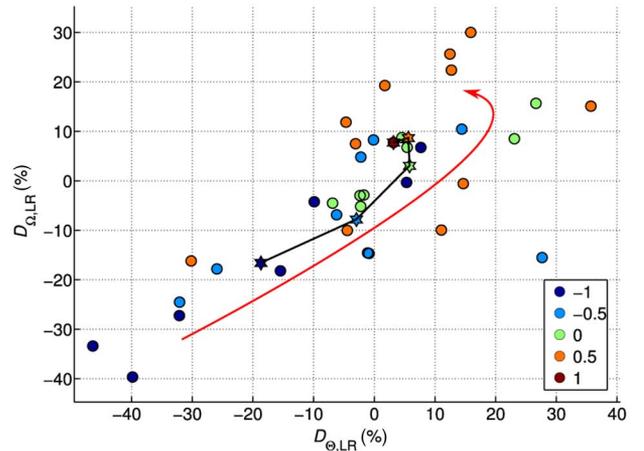

Fig. 10. Representation of average relative differences of amplitude-speed pairs between LLA and RLA $\{(D_{\Theta,\mathrm{LR},i}, D_{\Omega,\mathrm{LR},i})\}_{i=1}^{36}$ on the same plane. Pairs are colored according to the corresponding difference of UPDRS scores between the left and right legs. Centroids of each cluster of pairs (drawn as filled stars), corresponding to the same UPDRS score difference, are shown and are linked in ascending order from -1 to 1. For ease of clarity, a representative red arrow shows a smoothed version of this trajectory.

Focusing now on the joint analysis of the RLA and the LLA, in Fig. 10, the average relative differences of amplitude-speed pairs between LLA and RLA $\{(D_{\Theta,\mathrm{LR},i}, D_{\Omega,\mathrm{LR},i})\}_{i=1}^{36}$ are drawn on the same plane. As before, a clear trend is visible in the graph. Furthermore, it can be observed that low UPDRS scores are associated with pairs placed around (0,0). On the other hand, the highest differences in UPDRS scores correspond to pairs, which are distant from the (0,0) point, i.e., to LA tasks where significant differences between RLA and LLA emerge.

So far, it has been shown that there is a relationship between the UPDRS scores and the measured values of the kinematic variables. However, for ease of visualization, we have considered just pairs of variables. In order to overcome this limitation and consider all kinematic variables simultaneously, in [13], a principal component analysis (PCA) can be considered, in order to reduce the dimensionality of the measured data while still retaining most of the variance of the original data [19]. In [13], PCA is used to map the input five-dimensional (5-D) points $\{(\Theta_i, \Omega_i, P_i, R_i, F_i)\}_{i=1}^{72}$ into a lower-dimensional

space.[4] According to the results of the considered PCA, 87.8% of the original variance is retained by just using the first two components, whereas its 92.7% is retained by adding the third component. This shows, as expected, the presence of redundancy in the measured data. Such redundancy can be significantly reduced by just considering the original data projected onto 2-D or 3-D spaces, as determined by the PCA.

In order to evaluate the performance of an automatic detection system able to associate a measured set of kinematic values

---

[4]Note that, since different kinematic variable values have different magnitudes and ranges, before applying PCA, the original data are first centered at their means (which are set equal to 0) and rescaled to have a unit standard deviation.

to a specific UPDRS score, three methods have been considered: 1) nearest centroid classifier (NCC); k nearest neighbors (kNN); and (linear) support vector machine (SVM) [19]. For ease of clarity, though simple and standard implementations of the previous algorithms have been adopted,[5] a brief overview of the operational principles of these algorithms is now presented. In particular, given a new (unknown) sample point, the three considered classification methods act as follows.

1) The NCC method assigns the new point to the class with the nearest centroid—Euclidean distances between pairs of points are considered. To this end, centroids must be computed for all training samples of each class.

2) The kNN method assigns the new point to the class, which includes the majority of the kNN of the sample point—as for NCC, Euclidean distances between pairs of points are considered. Nearest neighbors are searched among all training samples. In the case of tie-breaks (i.e., when two or more classes contain the same number of samples among the kNN), the closest point is used to break the tie and its class is then chosen. Even if different values of k have been considered and evaluated, in the following, we will just consider the case with $k = 4$ (which, heuristically, appears to optimize the system performance).

3) The (linear) SVM method assigns the new point to the class associated with the decision region where the point lies. In order to define the decision regions, during a training phase, two classes at a time are considered and the hyperplanes, which maximize the separation between the training samples of the two classes are computed. Since, in this work, we deal with more than two classes, multiple training steps are performed. At each step, training samples of a given class are compared to the joint set of the training samples of the remaining classes: different hyperplanes and, consequently, multiple decision regions are then identified.

In order not to bias the performance of the classifiers, a leave-one-out cross-validation method is considered. This means that each point of the original dataset is used, in turn, as the new (unknown) point and the remaining points are used as a training dataset. The performance is then evaluated by averaging together the single observed performance results. We also define the absolute UPDRS error e as follows:

$$e \triangleq |\widehat{u} - u|$$

where u is the actual UPDRS score and $\widehat{u}$ is the estimated one (using NCC, kNN, or SVM).

In Fig. 11, all the pairs $\{(P_{X_\theta,i}, P_{X_\omega,i})\}_{i=1}^{72}$, which take into account the powers of the spectra of the frequency features introduced in Section III-C, are represented on the same plane. As for the previous figures, each pair is assigned a color corresponding to the related UPDRS score. Furthermore, the centroids (denoted by the filled stars) of each cluster of pairs, corresponding to the same UPDRS score, are also shown. Finally, the black line links the centroids from 0 to 3.5. Note
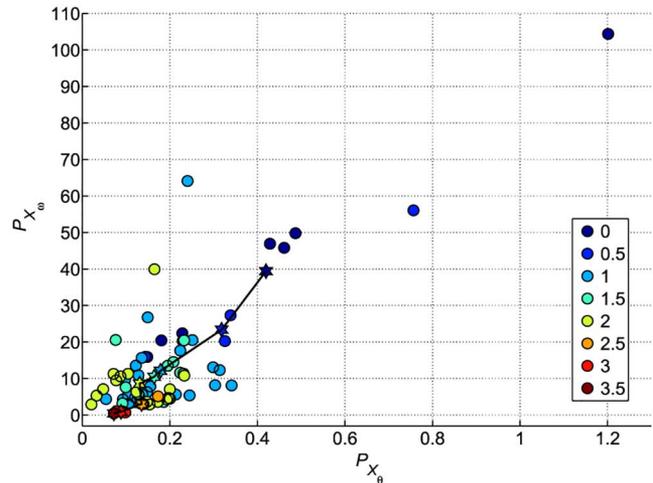
Fig. 11. Representation of pairs $\{(P_{X_\theta,i}, P_{X_\omega,i})\}_{i=1}^{72}$ on the same plane. Pairs are colored according to the corresponding UPDRS scores. Centroids of each cluster of pairs (drawn as filled stars), corresponding to the same UPDRS score, are shown and are linked in UPDRS-wise order from 0 to 3.5.

that, even if clusters of pairs corresponding to different UPDRS scores tend to overlap, a clear trend is visible showing that pairs mainly move from the upper right corner (i.e., the pairs with UPDRS 0) to the bottom part (i.e., the pair with UPDRS 3.5) of the plane.

In order to investigate the best performance achievable with the proposed system and with the considered features, an exhaustive performance analysis has been carried out, by testing: the system performance for all possible combinations of features; possible values of k (when the kNN method, which will turn out to be the best, is used); and the number of considered principal components (when PCA data are used, instead of original data). In particular,

1) the following 11 features, among those presented earlier, are selected: Θ, Ω, P, R, Θ_{SD}, Ω_{SD}, P_{SD}, R_{SD}, F, P_{X_ω}, and P_{X_θ};

2) when using the kNN method, the following values of k are considered: $1, 2, \ldots, 10$;

3) up to 11 principal components (as the number of features) are used when considering PCA data.

The three presented classifiers (namely, NCC, kNN, and SVM) have been run on both original data and "PCA-projected" data. In Fig. 12, a direct comparison of the cumulative distribution functions (cdfs) of e with NCC, kNN, and SVM is carried out. In particular, in Fig. 12(a), the cdfs for all possible combinations of parameters and features are shown using different colors for each classifier. It can be observed that the choice of the classifier, more than the choice of the features and parameters, is crucial in order to achieve good performance. Indeed, groups of cdfs for each classifier tend to lie in the same portion of the plane even for different features and parameters. To this end, in Fig. 12(b) the average cdfs (over all possible combinations of features and parameters) for each classifier are also shown. It is easy to observe that best performance can be achieved using kNN, followed by SVM and, eventually, NCC. Note also that performing the analysis on PCA data, rather than on original data, does not significantly improve the classifiers' performance. The best combination of features and
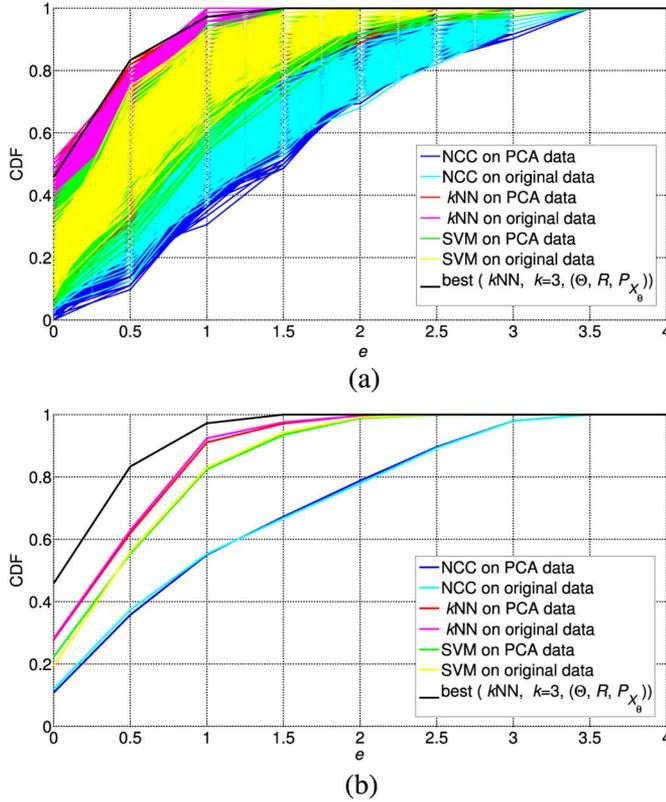
Fig. 12. CDFs of the absolute UPDRS error e using NCC, kNN, and SVM. The previous classifiers are used on both the original data and the PCA-projected data. In (a), the cdfs for all possible combinations of parameters and features are shown, whereas in (b), the average cdfs for every classifier are shown. The black solid line is the cdf of the best case (i.e., kNN with $k = 3$, using $(\Theta, R, P_{X_\theta})$ as features).
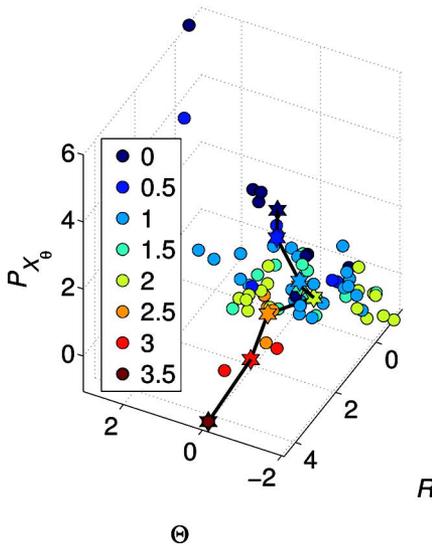

Fig. 13. Representation of 3-D points $\{\Theta_i, R_i, P_{X_\theta, i}\}_{i=1}^{72}$ on the same space. 3-D points are colored according to the corresponding UPDRS scores. Centroids of each cluster of points (drawn as filled stars), corresponding to the same UPDRS score, are shown and are linked in UPDRS-wise order from 0 to 3.5.

parameters, chosen as the one which maximize the area under the curve (AuC) of the cdfs, is resulted to be that which uses kNN with $k = 3$ and $(\Theta, R, P_{X_\theta})$ as features. In the previous figures, the black solid line represents the corresponding cdf.

For completeness, in Fig. 13, a trajectory, similar to the ones shown in Figs. 9–11, is drawn in the kinematic space of the best features. As for the previous bidimensional figures, in this case, as well a clear trajectory can be identified. This further confirms the feasibility of the design and implementation of an automatic UPDRS detection system.

V. CONCLUSION

In this paper, we have investigated how kinematic variables, collected through a simple BSN during the LA task, can be representative of the UPDRS value assigned by neurologists. We have first considered a "single-subject" perspective, trying to highlight similarities and differences between characteristic kinematic variables of a healthy subject and of a PD patient. Then, we have carried out a "large-scale" experimental investigation considering 24 PD patients. Many kinematic features, in both time and frequency domains, have been investigated, considering various classification methods (NCC, kNN, and SVM). The most representative ones have been characterized considering 2-D (amplitude-speed and amplitude power-speed power) and 3-D feature spaces (amplitude-amplitude power-regularity). In order to highlight the presence of correlation between the considered kinematic variables, a PCA has been carried out. However, our results show that using PCA-processed data, rather than original data, does not significantly improve the classifiers' performance. The best system configuration, chosen as the one which maximize the AuC of the cdfs of the decision error, turned out to be the one based on kNN with $k = 3$ and $(\Theta, R, P_{X_\theta})$ as features. In particular, characteristic "trajectories" (from low to high UPDRS scores) emerge in the considered multidimensional kinematic spaces, which is a promising result for the design of an automated UPDRS detection system, which could rely on the introduction of proper "UPDRS decision regions" in the considered kinematic spaces. Last, but not least, the use of a wireless BSN makes the proposed system directly integrable into IoT systems, paving the way to telerehabilitation applications and cloud computing-based processing of a large amount of heterogeneous data.

REFERENCES

[1] European Parkinson's Disease Association [Online]. Available: http://www.epda.eu.com/en/parkinsons/in-depth/parkinsonsdisease/
[2] B. Chen et al., "A web-based system for home monitoring of patients with Parkinsons disease using wearable sensors," IEEE Trans. Biomed. Eng., vol. 58, no. 3, pp. 831–836, Mar. 2011.
[3] S. Nuzik, R. Lamb, A. Vansant, and S. Hirt, "Sit-to-stand movement pattern: A kinematic study," Phys. Therapy, vol. 66, no. 11, pp. 1708–1713, 1986.
[4] D. Giansanti, G. Maccioni, F. Benvenuti, and V. Macellari, "Inertial measurement units furnish accurate trunk trajectory reconstruction of the sit-to-stand manoeuvre in healthy subjects," Med. Biol. Eng. Comput., vol. 45, no. 10, pp. 969–976, Oct. 2007.
[5] A. Salarian et al., "Gait assessment in Parkinson's disease: Toward an ambulatory system for long-term monitoring," IEEE Trans. Biomed. Eng., vol. 51, no. 8, pp. 1434–1443, Aug. 2004.
[6] A. Salarian et al., "Analyzing 180° turns using an inertial system reveals early signs of progression of Parkinsons disease," in Proc. 31st Annu. Int. Conf. IEEE Eng. Med. Biol. Soc. (EMBS), Minneapolis, MN, USA, Sep. 2009, pp. 224–227.
[7] A. Salarian et al., "Quantification of tremor and bradykinesia in Parkinson's disease using a novel ambulatory monitoring system," IEEE Trans. Biomed. Eng., vol. 54, no. 2, pp. 313–322, Feb. 2007.

[8] S. Fahn and R. L. Elton, "Unified Parkinson's disease rating scale," *Recent Developments in Parkinson's Disease*. Florham Park, NJ, USA: Macmillan, 1987, vol. 2, pp. 153–163.

[9] S. Patel *et al.*, "Monitoring motor fluctuations in patients with Parkinsons disease using wearable sensors," *IEEE Trans. Inf. Technol. Biomed.*, vol. 13, no. 6, pp. 864–873, Nov. 2009.

[10] S. Das *et al.*, "Quantitative measurement of motor symptoms in Parkinson's disease: A study with full-body motion capture data," in *Proc. 2011 Annu. Int. Conf. Eng. Med. Biol. Soc. (EMBC)*, 2011, pp. 6789–6792.

[11] D. A. Heldman *et al.*, "Automated motion sensor quantification of gait and lower extremity bradykinesia," in *Proc. 34th Annu. Int. Conf. IEEE Eng. Med. Biol. Soc. (EMBS)*, San Diego, CA, USA, Aug. 2012, pp. 1956–1959.

[12] M. Giuberti *et al.*, "On the characterization of leg agility in patients with Parkinson's disease," in *Proc. 10th Int. Conf. Wear. Implant. Body Sensor Netw. (BSN)*, Cambridge, MA, USA, May 2013, pp. 1–6.

[13] M. Giuberti *et al.*, "Linking UPDRS scores and kinematic variables in the leg agility task of Parkinsonians," in *Proc. 11th Int. Conf. Wear. Implant. Body Sensor Netw. (BSN)*, Zurich, Switzerland, Jun. 2014, pp. 115–120.

[14] A. Burns *et al.*, "SHIMMER: A wireless sensor platform for noninvasive biomedical research," *IEEE Sensors J.*, vol. 10, no. 9, pp. 1527–1534, Sep. 2010.

[15] R. B. Davis, S. Ounpuu, D. J. Tyburski, and J. R. Gage, "A gait analysis data collection and reduction technique," *Human Movement Sci.*, vol. 10, pp. 575–587, 1991.

[16] A. Ferrari *et al.*, "Quantitative comparison of five current protocols in gait analysis," *Gait Posture*, vol. 28, pp. 207–216, 2008.

[17] I. Y. Bar-Itzhack, "New method for extracting the quaternion from a rotation matrix," *J. Guidance Control Dynam.*, vol. 23, no. 6, pp. 1085–1087, Nov./Dec. 2000.

[18] S. O. H. Madgwick, A. J. L. Harrison, and R. Vaidyanathan, "Estimation of IMU and MARG orientation using a gradient descent algorithm," in *Proc. 2011 IEEE Int. Conf. Rehabil. Robotics (ICORR)*, Zurich, Switzerland, Jun. 2011, pp. 1–7.

[19] R. O. Duda, P. E. Hart, and D. G. Stork, *Pattern Classification and Scene Analysis*, 2nd ed. Hoboken, NJ, USA: Wiley-Interscience, 2000.

Matteo Giuberti (GSM'13–M'14) received the B.Sc. and M.Sc. degrees (*summa cum laude*) in telecommunications engineering and Ph.D. degree in information technologies from the University of Parma, Parma, Italy, in 2008, 2010, and 2014, respectively.

He is currently a Research Engineer with Xsens Technologies B.V., Enschede, The Netherlands. His research interests include data processing in wireless sensor networks (WSNs) and, more specifically, body sensor networks (BSNs), body area networks (BANs), inertial motion capture and posture recognition, motion reconstruction, activity classification, orientation estimation algorithms, telerehabilitation and mobile health applications, and wireless (indoor) localization.

Dr. Giuberti was the recipient of the first Body Sensor Network (BSN) Contest and ranked second in one task of the Opportunity Challenge in 2011. He was also the recipient of a Paper Award at BSN 2014.

Gianluigi Ferrari (S'96–M'98–SM'12) is currently an Associate Professor of telecommunications with the University of Parma, Parma, Italy. He was a Visiting Researcher with the University of Southern California (USC), Los Angeles, CA, USA, from 2000 to 2001, Carnegie Mellon University (CMU), Pittsburgh, PA, USA, from 2002 to 2004, King Mongkut's Institute of Technology Ladkrabang (KMITL), Bangkok, Thailand, in 2007, and Universit Libre de Bruxelles (ULB), Brussels, Belgium, in 2010. Since 2006, he has been the Coordinator with the Wireless Ad-Hoc and Sensor Networks (WASN) Laboratory, Department of Information Engineering, University of Parma. His research interests include wireless *ad-hoc* and sensor networking, adaptive digital signal processing, and communication theory.

Prof. Ferrari currently serves on the Editorial Board of several international journals. He was the recipient of the Paper/Technical Awards at IWWAN06, EMERGING10, BSN 2011, ITST-2011, SENSORNETS 2012, EvoCOMNET 2013, BSN 2014, and SoftCOM 2014.

Laura Contin is a Senior Researcher with the Strategy and Innovation Department, Telecom Italia, Turin, Italy. She has researched and published extensively in multimedia telecommunications, and is currently involved in R&D projects related to active aging, remote rehabilitation, and remote monitoring of neurological patients. She has authored numerous international conference papers, journal papers, and patents. Her research interests include body sensor networks, algorithms for motion tracking, and ambient assisted living.

Veronica Cimolin received the Master's and Ph.D. degrees in bioengineering (with a focus on the quantitative analysis of movement for the assessment of functional limitation in children with Cerebral Palsy), from the Politecnico di Milano, Milan, Italy, in 2002 and 2007, respectively.

Currently, she is a Researcher with the Department of Electronics, Information, and Bioengineering, Politecnico di Milano. She is with the "Luigi Divieti" Posture and Movement Analysis Laboratory. She is involved in the activity of several movement analysis laboratories of national and international institutes. She teaches the course "Impianti ospedalieri e sicurezza" and assists in the teaching of "Laboratorio di valutazione funzionale." She has authored several peer-reviewed international papers. Her research interests include quantitative movement analysis for clinical and rehabilitative applications.

Corrado Azzaro received the M.D. degree in medicine and surgery from the University of Palermo, Palermo, Italy, in 2002.

He completed his specialty training in clinical neurology with the Neurology Department, "Molinette Hospital," Turin, Italy, in 2011. He has been a Visiting Doctor with the "Centro de evaluacin neurologica para nios y adolecentes" (CENNA), Monterrey, Mexico, from 2002 to 2003, and with the Neurology Department, "Hospital Virgen del Rocio," Sevilla, Spain, in 2003. He is currently as an Assistant with the Department of Neurology, "San Giuseppe" Hospital, Clinical Research Institute "Istituto Auxologico Italiano," Piancavallo, Verbania, Italy. His research interests include neurophysiology, movement analysis in virtual reality environments, and applied medical informatics.

Giovanni Albani received the M.D. degree in medicine and surgery from the University of Pavia, Pavia, Italy, in 1992, and completed the School of Neurophysiopathology, Neurological National Institute "Casimiro Mondino," Pavia, Italy, in 1997.

He has been a Visiting Researcher with the Hospital Clinico (1990) and Bellvitge, Barcelona, Spain (1992), and Neurologische Clinic University of Zurich, "Paul Sherrer Institute" Nuclear Medicine Centre Villigen, Switzerland, and "Balgrist" Swiss Paraplegic Zentrum, Zurich, Switzerland (from 1995 to 1997). After being Chief of Service of Neurophysiology in Clinical Hospital "Beato Matteo," Vigevano, Italy (1998–2005). He is currently an Assistant with the Department of Neurology, "San Giuseppe" Hospital, Clinical Research Institute "Istituto Auxologico Italiano," Piancavallo-Verbania, Italy. His research interests include movement disorders, movement analysis, neurophysiology, and virtual reality.

Alessandro Mauro is a Full Professor of neurology with the Department of Neurosciences, Medical School, University of Torino, Turin, Italy, since 2007. Since 2000, he has been the Medical Director with the University Unit of Neurology and Neurorehabilitation, and with the Laboratory of Neuropathology and Clinical Neurobiology, San Giuseppe Hospital—Istituto Auxologico Italiano—IRCCS, Piancavallo-Oggebbio (VB), Italy. Since 2010, he has been the Medical Director with the Centre of Sleep Medicine of the same institution. His research interests include clinical neurology, neurogenetics and molecular neuropathology of neurodegenerative diseases, neurorehabilitation, and sleep disorders.

Prof. Mauro is an active Member of National and International Scientific Societies, including, the Italian Association of Neuropathology and Clinical Neurobiology (AINPeNC) of which he was the President from 2011 to 2013 (current past-president and a Member of the Board of Governors).